Water-Soluble Aromatic Nanobelt with Unique Cellular Internalization

Konstantin Günther,[a,b] Hideya Kono,[a] Hiroki Shudo,[a] Reika Isoda,[c] Masayoshi Nakamura,[c] Akiko Yagi,*[a,c] Kazuma Amaike,*[d] and Kenichiro Itami*[c,d]

[a] K. Günther, H. Kono, Dr. H. Shudo, Prof. Dr. A. Yagi, Prof. Dr. K. Amaike
Department of Chemistry, Graduate School of Science,
Nagoya University,
Chikusa, Nagoya 464-8602, Japan
E-mail: yagi.akiko@itbm.nagoya-u.ac.jp (A.Y.), amaike.kazuma.s9@f.mail.nagoya-u.ac.jp (K.A.)

[b] K. Günther
Department of Chemistry,
Humboldt-Universität zu Berlin,
Brook-Taylor-Straße 2, 12489 Berlin, Germany

[c] Dr. R. Isoda, Prof. Dr. M. Nakamura, Prof. Dr. A. Yagi, Prof. Dr. K. Itami
Institute of Transformative Bio-Molecules (WPI-ITbM),
Nagoya University,
Chikusa, Nagoya 464-8602, Japan

[d] Prof. Dr. K. Itami
Molecule Creation Laboratory, RIKEN Cluster for Pioneering Research,
RIKEN,
Wako, Saitama 351-0198, Japan
E-mail: kenichiro.itami@riken.jp (K.I.)

Supporting information for this article is given via a link at the end of the document.

Abstract: A water-soluble aromatic nanobelt was synthesized, and its cellular uptake behavior in HeLa cells was investigated. The late-stage functionalization of the parent methylene-bridged [6]cycloparaphenylene ([6]MCPP) provided an easily accessible alkyne-functionalized nanobelt in a single reaction step. The alkyne-substituted [6]MCPP was subjected to Cu-catalyzed azide–alkyne cycloaddition by using a dye-attached azide to obtain a water-soluble aromatic nanobelt. Cell-imaging experiments on the synthesized nanobelt in HeLa cells revealed stop-and-go cellular uptake dynamics. Similar experiments with control molecules and theoretical studies indicated that the unique dynamics of the nanobelt was derived from the belt-shaped structure.

Aromatic nanobelts and carbon nanorings have attracted considerable attention as synthetic targets because of their interesting chemical structures and desirable physical properties.[1] Since the first synthesis of cycloparaphenylenes (CPPs) by Bertozzi and Jasti in 2008[2] and our size-selective synthesis of [12]CPP in 2009,[3] several CPP derivatives have been synthesized and their unique size-dependent properties revealed.[4] In 2017, we successfully synthesized the first fully fused and aromatic nanobelt, the (6,6)carbon nanobelt (CNB),[5] followed by the (8,8)CNB and (12,12)CNB.[6] Subsequently, various CNBs were synthesized, thereby opening up a new field of aromatic nanobelt science.[7] In 2020, we fabricated a new nanobelt, namely methylene-bridged [6]cycloparaphenylene ([6]MCPP), by performing six-fold intramolecular aryl–aryl coupling of a pillar[6]arene-based precursor.[8]

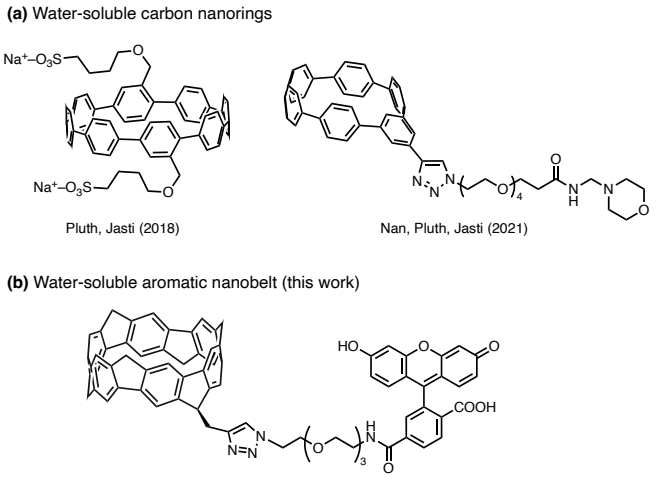

Figure 1. (a) Water-soluble carbon nanorings reported by Pluth et al. and Nan et al. (b) Water-soluble aromatic nanobelt synthesized via late-stage functionalization in this work.

The interesting physical properties of carbon nanorings have led to various applications,[9] particularly in the biological field. However, hydrophilic moieties must be introduced because the carbon nanoring structures are inherently highly hydrophobic. In a pioneering study, Pluth and Jasti synthesized a water-soluble [8]CPP by introducing clickable substituents as a biocompatible fluorophore during the initial step of synthesis (Figure 1a).[10] In 2021, Nan, Pluth, and Jasti reported a water-soluble *meta*[6]CPP for targeting subcellular proteins (Figure 1a).[11] In these previous studies, the introduction of functional groups at an early stage of synthesis and the use of protection groups, which lead to multistep syntheses, were often needed. The introduction of water-soluble moieties into carbon nanorings can be avoided by

dispersing nanorings that are insoluble in water with lipids, surfactants, and water-soluble organic solvents for bioimaging.[12] Although various bioimaging applications have been reported for carbon nanorings, none have been reported thus far for nanobelts having unique characteristics such as rigidity and an internal space with fixed benzene rings. Herein, we report the first synthesis of a water-soluble aromatic nanobelt via late-stage functionalization and investigate its dynamics in HeLa cells (Figure 1b).

First, we synthesized a water-soluble aromatic nanobelt (**1**; Scheme 1). To fabricate readily available molecules, synthesis must be straightforward. We envisioned that commercially available [6]MCPP (**3**)[8] can be functionalized in a single reaction step owing to its reactive benzylic methylene bridge. We selected an alkyne moiety as the substituent because of its easy accessibility to the desired functionalization via click reactions. Thus, **3** was treated with KO*t*-Bu in dimethylformamide (0 °C and 5 min) and then with propargyl bromide (0 °C and 5 min). This well-controlled deprotonation/S_N2 reaction resulted in alkyne-functionalized [6]MCPP (**2**) in 27% yield (Scheme 1). Higher substitution products were separated from **2** by applying recycling gel permeation chromatography. Notably, under harsh reaction conditions, such as deprotonation/S_N2 reactions at high temperatures and/or long reaction times, the decomposition of [6]MCPP and multi-propargylation occur. Propargylation occurred at the outer methylene hydrogen atom (H_{out}), likely owing to steric hindrance. The optical properties of **2** were similar to those of the parent nanobelt (**3**), illustrating that the nanobelt scaffold was not perturbed upon the substitution of the methylene bridge (Figures S4–S6). Finally, copper(I)-catalyzed azide–alkyne cycloaddition of **2** with 6-FAM-PEG3-azide, which is a fluorescent dye, resulted in the desired water-soluble aromatic nanobelt (**1**) in 6% yield. The optical properties derived from the [6]MCPP scaffold in nanobelts **1** and **2** were similar to those in **3**, illustrating that the nanobelt scaffold was not perturbed upon the substitution of the methylene bridge (Figures S7–S9). In particular, the molar absorption coefficient of the MCPP scaffold in **1** (ε ≈ 40,000) did not differ significantly from those in **2** and **3**, and at long wavelengths, no gentle bands appeared to aggregate, suggesting that **1** was sufficiently soluble in water.

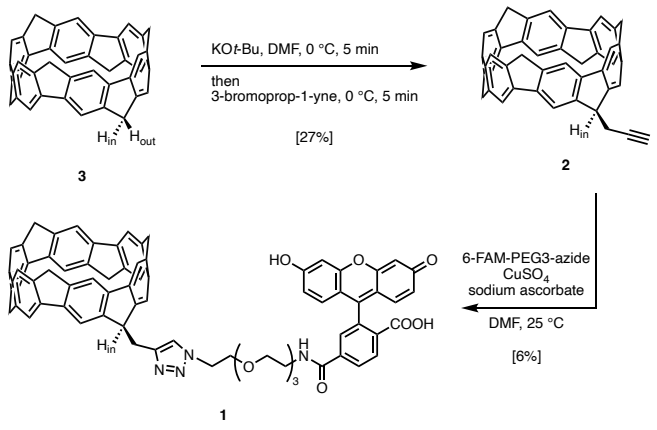

Scheme 1. Synthesis of a water-soluble aromatic nanobelt (**1**). 6-FAM-PEG3-azide = *N*-[2-[2-[2-(2-azidoethoxy)ethoxy]ethoxy]ethyl]-3',6'-dihydroxy-3-oxo-3*H*-spiro[isobenzofuran-1,9'-xanthene]-6-carboxamide.

We demonstrated the bioimaging of the water-soluble aromatic nanobelt (**1**). To better understand the structure–property relationship, control compounds **4** and **5**, having a fluorene unit, the partial structure of **1**, or almost the same log P value[13] as **1** (**1**: 5.98, **5**: 6.12), were also synthesized (Figure 2a). Thus, HeLa cells were incubated with 10 μM of each compound in a culture medium with fetal bovine serum (FBS) for 24 h (Figure 2b). Confocal microscopy images showed that the fluorescence of nanobelt **1** was diffusely distributed within the cells and lacked localization to specific cell organelles, even though compound **5** was detected in the cell membrane. In contrast, compound **4** did not show cell permeability. To investigate the dynamics in detail, the incubation time of the compounds was adjusted to either 30 min or 2 h. After 30 min of incubation, nanobelt **1** was mainly observed in the cell membrane; however, after 2 h of incubation, nanobelt **1** was diffusely distributed within the cells and lacked localization to specific cell organelles (Figure 2c). Compound **5** was localized in the cell membrane after both 30 min and 2 h of incubation (Figure S12). Nevertheless, the dynamics with and without FBS differed between compounds **1** and **5**. Nanobelt **1** showed higher fluorescence intensity in the absence than in the presence of FBS, with no change in dynamics (Figure 2d). In contrast, compound **5** showed membrane localization in the presence of FBS but was present in the cytoplasm in the absence of FBS (Figure S13). These drastic changes in compound **5** in the presence or absence of FBS suggested that compound **5** was closely related to biological activities such as metabolism (Figure S14). The dynamics of **1** seemed to originate from its unique belt-shaped structure and not from its hydrophobicity and fluorene structure. We hypothesized that these unexpected effects of **1** in cells were due to interactions between **1** and biomolecules, such as proteins.

To gain insight into the molecular dynamics mechanisms of **1** within cells, we estimated the interactions between *N*- and *C*-protected amino acids and [6]MCPP by performing density functional theory (DFT) calculations (Figure 3). The small diameter of the [6]MCPP cavity (approximately 7.8 Å) indicated a preference for forming host–guest complexes with small and less branched amino acids.[14] Using the B3LYP-GD3/6-31G(d) level of theory and the counterpoise method, we calculated the stabilization energies of complexes involving methionine, glutamine, glutamic acid, lysine, and alanine under pH-neutral conditions (pH = 7.4). Under these conditions, glutamic acid functioned as a monovalent anion, whereas lysine acted as a monovalent cation. The resultant stabilization energies for interactions with [6]MCPP were estimated to be 21.5, 35.9, 25.1, 53.7, and 16.1 kcal/mol for methionine, glutamine, glutamic acid, lysine, and alanine, respectively. The exceptionally high complexation energy with cationic lysine highlighted the potential significant contribution of cation-π interactions in the binding processes between **1** and proteins. Although further detailed studies are needed to fully understand the underlying mechanisms, these findings suggested a robust potential for **1** to interact with proteins. The observed reduction in the fluorescence intensity of **1** in the presence of FBS could be due to interactions with albumin in FBS (Figures 2c and 2d). Furthermore, **1** likely localized to the cell membrane through interactions with

membrane proteins and subsequently localized within the cytoplasm through interactions with cytoplasmic proteins. The X-ray crystal structure of [6]MCPP, with hexane captured in its cavity,[8] indicated a potential interaction between [6]MCPP and lipids. Another possible mechanism underlying the membrane localization of **1** is the interaction with lipids in the plasma membrane (Figure 4).

In summary, we successfully synthesized and characterized the first water-soluble aromatic nanobelt (**1**). We presented alkyne-functionalized [6]MCPP (**2**) as a key synthetic intermediate that can serve as a platform for highly functionalized nanobelts; it was conveniently synthesized in a single reaction step via late-stage functionalization from [6]MCPP (**3**). Confocal fluorescence microscopy experiments on **1** demonstrated the unique topological role of nanobelts in biological systems. Additionally, our DFT calculations revealed interactions between [6]MCPP and certain amino acids, with a notable binding affinity for cationic lysine, thereby indicating significant potential for protein interactions. A range of bio-applications using water-soluble aromatic nanobelts are currently underway in our laboratory.

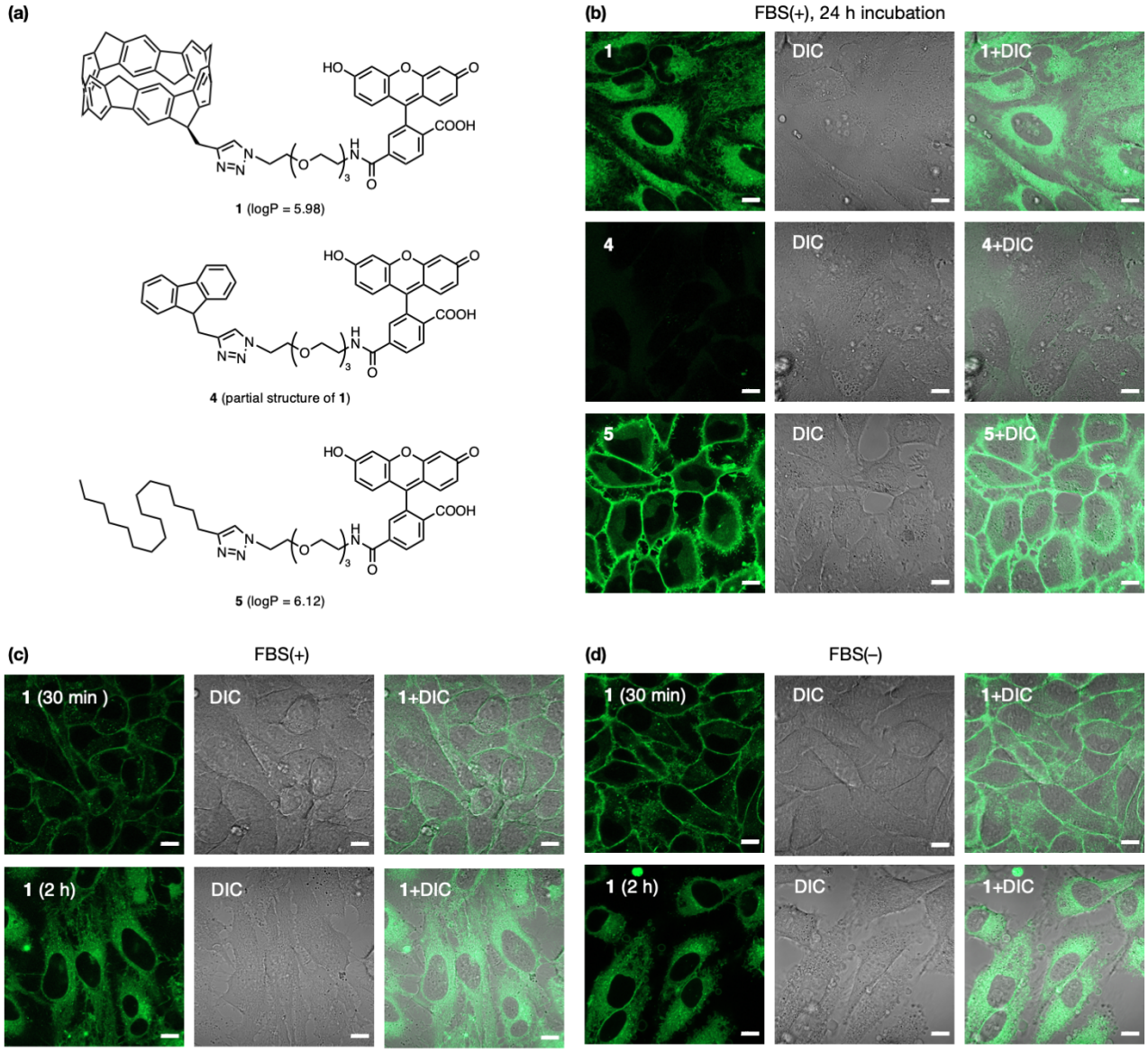

Figure 2. (a) Structures of compounds **1**, **4**, and **5**. (b) Fluorescence and digital image correlation (DIC) images of HeLa cells incubated with **1**, **4**, and **5** for 24 h in the presence of FBS. Fluorescence and DIC images of HeLa cells incubated with **1** for 30 min or 2 h (c) in the presence of FBS and (d) in the absence of FBS. Scale bars at 10 μm.

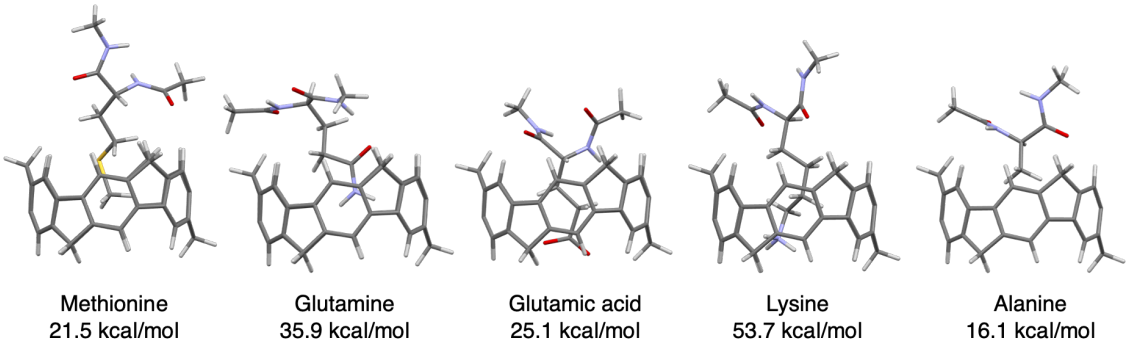

Figure 3. Host–guest complexes formed between [6]MCPP and selected amino acid side chains. The carboxylic acid and amine groups of the amino acids were amidated to simulate the environment of the amino-acid side chains. Level of theory: B3LYP-GD3/6-31G(d)

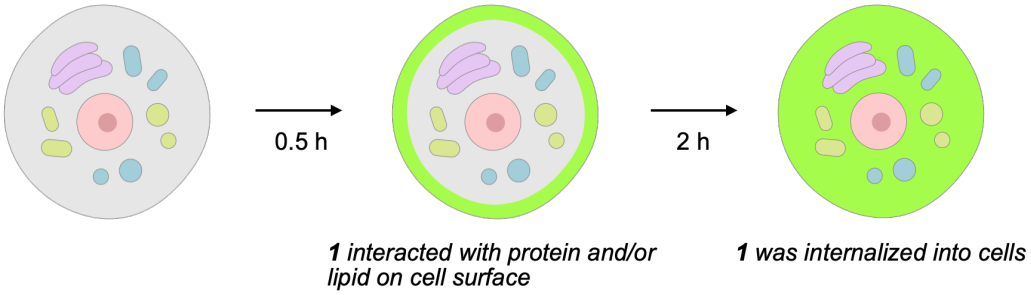

Figure 4. Plausible mechanism for the internalization of nanobelt **1**

Acknowledgements

This work was supported by Uehara Memorial Foundation (to K.I.), Chugai Foundation for Innovative Drug Discovery Science (to K.I.), and JSPS Promotion of Joint International Research (grant number 22K21346 to A.Y.). K.G. was supported by a PROMOS scholarship from the German Academic Exchange Service (DAAD) and Humboldt University, Berlin. H.K. and H.S. acknowledge the JSPS Fellowship for Young Scientists. Computations were performed at the Research Center for Computational Science, Okazaki, Japan (Project: 23-IMS-C987, 24-IMS-C117). We thank Mr. Daisuke Shimizu for assistance with cell culture.

Conflict of Interest

The authors declare no conflict of interest.

Data Availability Statement

The data that support the findings of this study are available in the Supporting Information of this article.

Keywords: aromatic compounds • bioimaging • cycloparaphenylene • late-stage functionalization • nanobelt

[1] a) S. E. Lewis, *Chem. Soc. Rev*. **2015**, *44*, 2221–2304; b) Y. Segawa, A. Yagi, K. Matsui, K. Itami, *Angew. Chem. Int. Ed.* **2016**, *55*, 5136–5158; c) Q. H. Guo, Y. Qiu, M. X. Wang, J. F. Stoddart, *Nat. Chem.* **2021**, *13*, 402–419; d) D. Imoto, A. Yagi, K. Itami, *Precis. Chem*. **2023**, *1*, 516–523.

[2] R. Jasti, J. Bhattacharjee, J. B. Neaton, C. R. Bertozzi, *J. Am. Chem. Soc.* **2008**, *130*, 17646–17647.

[3] H. Takaba, H. Omachi, Y. Yamamoto, J. Bouffard, K. Itami, *Angew. Chem. Int. Ed.* **2009**, *48*, 6112–6116.

[4] a) Y. Segawa, A. Fukazawa, S. Matsuura, H. Omachi, S. Yamaguchi, S. Irle, K. Itami, *Org. Biomol. Chem.* **2012**, *10*, 5979–5984; b) E. R. Darzi, R. Jasti, *Chem. Soc. Rev.* **2015**, *44*, 6401–6410; c) C. Camacho, T. A. Niehaus, K. Itami, S. Irle, *Chem. Sci.* **2013**, *4*, 187–195.

[5] G. Povie, Y. Segawa, T. Nishihara, Y. Miyauchi, K. Itami, *Science* **2017**, *356*, 172–175.

[6] G. Povie, Y. Segawa, T. Nishihara, Y. Miyauchi, K. Itami, *J. Am. Chem. Soc.* **2018**, *140*, 10054–10059.

[7] a) K. Y. Cheung, K. Watanabe, Y. Segawa, K. Itami, *Nat. Chem.* **2021**, *13*, 255–259; b) Y. Segawa, T. Watanabe, K. Yamanoue, M. Kuwayama, K. Watanabe, J. Pirillo, Y. Hijikata, K. Itami, *Nat. Synth.* **2022**, 1–7; c) K. Y. Cheung, S. Gui, C. Deng, H. Liang, Z. Xia, Z. Liu, L. Chi, Q. Miao, *Chem* **2019**, *5*, 838–847; d) Z. Xia, S. H. Pun, H. Chen, Q. Miao, *Angew. Chem. Int. Ed.* **2021**, *133*, 10399–10406; e) H. M. Bergman, G. R. Kiel, R. C. Handford, Y. Liu, T. D. Tilley, *J. Am. Chem. Soc.* **2021**, *143*, 8619–8624; f) S. Nishigaki, Y. Shibata, A. Nakajima, H. Okajima, Y. Masumoto, T. Osawa, A. Muranaka, H. Sugiyama, A. Horikawa, H. Uekusa, *J. Am. Chem. Soc.* **2019**, *141*, 14955–14960.

[8] a) Y. Li, Y. Segawa, A. Yagi, K. Itami, *J. Am. Chem. Soc.* **2020**, *142*, 12850–12856; b) H. Kono, Y. Li, R. Zanasi, G. Monaco, F. F. Summa, L. T. Scott, A. Yagi, K. Itami, *J. Am. Chem. Soc.* **2023**. *145*, 8939–8946.

[9] a) N. Ozaki, H. Sakamoto, T. Nishihara, T. Fujimori, Y. Hijikata, R. Kimura, S. Irle, K. Itami, *Angew. Chem. Int. Ed.* **2017**, *56*, 11196–11202; b) P. Della Sala, N. Buccheri, A. Sanzone, M. Sassi, P. Neri, C. Talotta, A. Rocco, V. Pinchetti, L. Beverina, S. Brovelli, *Chem. Commun.* **2019**, *55*, 3160–3163; c) E. J. Leonhardt, J. M. Van Raden, D. Miller, L. N. Zakharov, B. Alemán, R. Jasti, *Nano Lett.* **2018**, *18*, 7991–7997; d) S. Canola, C. Graham, Á. J. Pérez-Jiménez, J.-C. Sancho-García, F. Negri, *Phys. Chem. Chem. Phys.* **2019**, *21*, 2057–2068; e) L. Hu, Y. Guo, X. Yan, H. Zeng, J. Zhou, *Phys. Lett. A* **2017**, *381*, 2107–2111; f) E. Kayahara, L. Sun, H. Onishi, K. Suzuki, T. Fukushima, A. Sawada, H. Kaji, S. Yamago, *J. Am. Chem. Soc.* **2017**, *139*, 18480–18483.

[10] B. M. White, Y. Zhao, T. E. Kawashima, B. P. Branchaud, M. D. Pluth, R. Jasti, *ACS Cent. Sci.* **2018**, *4*, 1173−1178.

[11] T. C. Lovell, S. G. Bolton, J. P. Kenison, J. Shangguan, C. E. Otteson, F. Civitci, X. Nan, M. D. Pluth, R. Jasti, *ACS Nano* **2021**, *15*, 15285–15293.

[12] a) H. Tang, Z. Gu, C. Li, Z. Li, W. Wu, X. Jiang, *Biomater. Sci.* **2019**, *7*, 2552–2558; b) Z.-L. Qiu, M.-b. He, K.-S. Chu, C. Tang, X.-W. Chen, L. Zhu, L.-P. Zhang, D. Sun, J. Qian, Y.-Z. Tan, *Adv. Opt. Mater.* **2021**, *9*, 2100482; c) Y. K. Park, Y. Huh, D. Kim, *Dyes Pigm.* **2023**, *211*, 111056; d) H. Chen, M. Shao, H. Li, H. Liu, W.-M. Wei, R.-H. Zheng, M. Song, R. Liu, D. Lu, *New J. Chem.* **2022**, *46*, 16670–16674.

[13] I. V. Tetko, V. Y. Tanchuk, *J. Chem. Inf. Comput. Sci.*, **2002**, *42*, 1136–1145.

[14] a) C. Huang, Y. Huang, N. G. Akhmedov, B. V. Popp, J. L. Petersen, K. K. Wang, *Org. Lett.* **2014**, *16*, 2672–2675; b) D. Lu, G. Zhuang, H. Jia, J. Wang, Q. Huang, S. Cui, P. Du, *Org. Chem. Front.* **2018**, *5*, 1446–1451; c) N. Grabicki, K. T. Nguyen, S. Weidner, O. Dumele, *Angew. Chem. Int. Ed.* **2021**, *60*, 14909–14914; d) N. Grabicki, S. Fisher, O. Dumele, *Angew. Chem. Int. Ed.* **2023**, *62*, e202217917.

Entry for the Table of Contents

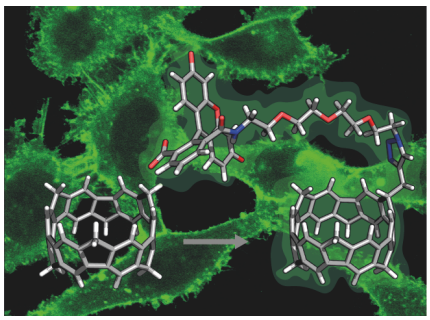

A water-soluble aromatic nanobelt was synthesized by the late-stage functionalization of [6]MCPP. Cell-imaging experiments on the synthesized nanobelt in HeLa cells revealed stop-and-go cellular uptake dynamics, which are likely derived from the belt-shaped structure.

Institute and/or researcher Twitter usernames: @Itamilab, @yagiakiko1